Assessment of a noninvasive optical photoplethysmography imaging device with dynamic tissue phantom models

C. Ikenna Nwafor
Kevin D. Plant
Darlene R. King
Brian P. McCall
John J. Squiers
Wensheng Fan
J. Michael DiMaio
Jeffrey E. Thatcher

SPIE.

Assessment of a noninvasive optical photoplethysmography imaging device with dynamic tissue phantom models

C. Ikenna Nwafor,[a] Kevin D. Plant,[a] Darlene R. King,[a] Brian P. McCall,[a] John J. Squiers,[a,b,c] Wensheng Fan,[a] J. Michael DiMaio,[a,c] and Jeffrey E. Thatcher[a,*]
[a]Spectral MD, Inc., Texas, United States
[b]Baylor University Medical Center, Department of Surgery, Texas, United States
[c]Baylor Research Institute, Baylor Scott and White Health, Texas, United States

Abstract. Noncontact photoplethysmography (PPG) has been studied as a method to provide low-cost, non-invasive, two-dimensional blood oxygenation measurements and medical imaging for a variety of near-surface pathologies. To evaluate this technology in a laboratory setting, dynamic tissue phantoms were developed with tunable parameters that mimic physiologic properties of the skin, including blood vessel volume change, pulse wave frequency, and tissue scattering and absorption. Tissue phantoms were generated using an elastic tubing to represent a blood vessel where the luminal volume could be modulated with a pulsatile fluid flow. The blood was mimicked with a scattering and absorbing motility standard, and the tissue with a gelatin–lipid emulsion hydrogel. A noncontact PPG imaging system was then evaluated using the phantoms. Noncontact PPG imaging accurately identified pulse frequency, and PPG signals from these phantoms suggest that the phantoms can be used to evaluate noncontact PPG imaging systems. Such information may be valuable to the development of future PPG imaging systems. © *2017 Society of Photo-Optical Instrumentation Engineers (SPIE)* [DOI: 10.1117/1.JBO.22.9.096003]

1 Introduction

Optical imaging methods can provide rapid and noninvasive assessments of wounds to aid in clinical decision making such as the evaluation of decubitus ulcers, skin flaps, and burn wounds, among other pathologies.[1–4] The optical pathway of light through the skin facilitates the examination of near-surface physiology, including microcirculation of blood through the dermal and epidermal layers. The ability to detect blood flow and to evaluate abnormal circulation or oxygen content patterns across a tissue's surface allows clinicians to measure relative tissue viability—a key piece of data for healthcare providers managing wounds. Recently, noncontact photoplethysmography (PPG) systems have shown promise in the assessment of blood flow across large surface areas. Noncontact PPG systems map blood flow with a potentially faster response time.[5] However, this measurement cannot be obtained without overcoming several practical obstacles. These include the spatial relationship among the light source, photodetector, and tissue, the stability of the camera and patient, intensity and color of emitted light, and presence of ambient light.[6] Isolating the physiologic variables from these signal measurement variables can be difficult during sensor engineering and testing of signal processing algorithms. Further development of these imaging systems requires tunable testing environments for assessing the performance of the systems.

Tissue-like phantoms exist for many imaging modalities, and they serve as tissue-simulating media that mimic the properties of human and animal tissues. These phantoms are used for a variety of purposes, including initial testing of system designs, optimization of signal-to-noise ratio (SNR), routine quality control, and comparison of performance among systems.[7] The key to developing useful phantoms is understanding the physical and optical properties the imaging system assesses then simulating them. Very few phantoms exist for assessing PPG systems due to the difficultly in replicating the physiologic parameters of the PPG signal.[8]

Noncontact PPG imaging systems are comprised of an illumination source and image sensor arranged in a reflective mode, on the same side of the tissue. Noncontact optical PPG measurements are generated by detecting the oscillating volume change in superficial tissue components, such as the arterioles in the skin, by measuring the interactions between tissue and incident photons.[5,9] Both the absorptive and scattering properties of tissue are altered during the cardiac cycle, affecting the pathway of light through the skin and its degree of absorbance.[10] Pulsing arterial blood flow in viable human tissue, realized as both an increase in arterial luminal diameter and an increase in tissue–blood concentration during systole, accounts for a 1% to 2% alternating current (AC) in light absorbance above the constant absorbance of the tissue.[11] Therefore, photon interaction with this change in blood concentration can be detected by an increase in path length as well as an increase in absorbance due to the higher concentration of absorbent heme-containing proteins during systole. The PPG signal intensity oscillates with the changing interaction of light transmitted through tissue as the volume of blood increases and decreases with the pulse pressure.[12] The effects of other important physiologic activities, such as respiration and sympathetic nervous activation, on the

---

*Address all correspondence to: Jeffrey E. Thatcher, E-mail: thatcher@spectralmd.com

peripheral circulation can be identified in the *in vivo* PPG signal as well. The experiment made use of a tissue phantom model, so there would be no evidence of these physiologic activities in the PPG system. In addition to AC modulation, important characteristics of the PPG signal include the direct current (DC) offset, frequency, and characteristic shape.

The development of more complex phantoms has increased along with the interest in applications of light and imaging in medicine,[7] and given the utility of tissue phantoms, it is important the phantoms are accurate and widely available. Absorption and scattering are the two key optical properties of human tissue and are often replicated in tissue phantoms. To reproduce the scattering characteristics observed in tissues, milk, lipids, TiO_2, Al_2O_3, and polymer microspheres are often used, while India ink, molecular dyes, and fluorophores are the primary absorbers.[7] These materials are well known and available, having been used in previously developed phantoms. The utility of a phantom is primarily determined by the matrix material. Common substances used to create the tissue phantom matrix are aqueous suspension, gelatin, polyacrylamide, or silicone.[7] Some are rigid materials that allow creation of solid, durable structures. Others are fluid and flexible, allowing for malleability and the addition of various optical components.

For the development of a viable PPG tissue phantom, not only were optical scattering and absorbance necessary but also the creation of a 1%- to 2%-luminal volume change was key. This vessel volume change is responsible for the creation of the PPG signal, and current tissue phantoms have not been able to replicate this physiology. Using widely available components, we developed phantoms that have tissue-like volume changes at frequencies comparable to the human heart rate. We assessed their ability to generate these physiological parameters. We then used a noncontact PPG imaging system to identify these same physiological parameters.[13] Ultimately, the bench tests used in these experiments demonstrated the ability of the noncontact PPG system to detect pulsatile flow in the dynamic phantoms. The phantoms produced would be valuable in the assessment of future PPG imaging systems.

2 Methods

2.1 Optical Phantoms

Optical bare-vessel and tissue phantoms that mimic physiological circulation with artificial PPG signals were developed as described in Secs. 2.1.1–2.1.3.

2.1.1 Motility standard

The motility standard was an aqueous solution containing two components selected to simulate the optical properties of scattering and absorbance that characterize the interaction of blood with light in the near-infrared (NIR) range. The motility standard was comprised of 0.2% 100-nm polystyrene beads (Sigma-Aldrich, St. Louis, Missouri) and 0.1% India ink (Higgins Inks, Leeds, Massachusetts) manually mixed in deionized water.[14] India ink was used to simulate NIR absorbance because it interacts with the incident NIR light in a manner similar to hemoglobin.

2.1.2 Bare-vessel phantoms

Bare-vessel phantoms were generated by positioning four segments of 1.58-mm inner-diameter silastic tubing (Dow Corning,

Midland, Michigan) such that they lay parallel at distances of 1, 5, and 10 mm apart. Silastic tubing was chosen because it was readily available, optically clear, and demonstrated elasticity similar to that of human arterial vessels, with a Young modulus of 2.1 MPa at 200% elongation.[15] The motility standard was placed inside the tubing and pumped with a two-roller peristaltic pump (Watson Marlow, Wilmington, Massachusetts; Model# sciQ32) at varying frequencies to generate pulsatile fluid flow. The pump was capable of producing pulse frequencies over the physiologic range of the human heartbeat [40 to 200 beats per minute (bpm)].[16,17] The pressure of the fluid was measured directly with the calibrated digital pressure transducer (calibrated against a Dwyer Series 490 digital manometer) and recorded using LabVIEW software (Signal Express, version 2.5).

In order to determine the pump pressure that provided a 2% luminal volume change consistent with physiologic tissue-volume changes during the cardiac cycle,[15,18,19] a section of the silastic tubing was filled with a 2% India ink solution and examined under a microscope to measure the diameter change that occurred with various pump pressures. The change in the cross sectional area of the inner lumen of the tube was linearly correlated with pump pressure (Table 1; $R^2 = 0.9826$). This result demonstrated that under the range of pressures tested, the silastic tubing remained in the elastic region of its stress–strain relationship. A pressure change of 150 mmHg provided the diameter change that resulted in the desired 2% lumen volume change, which is essential for a PPG imaging system.

2.1.3 Tissue phantoms

Tissue phantoms were comprised of a gelatin–lipid solution molded around the silastic tubing. The tissue phantoms were designed to model the characteristic absorbance and scattering observed during light's interaction with skin. In skin tissue, light absorption is primarily dependent upon hemoglobin and is therefore proportional to the volume fraction of whole blood. In humans, the average volume fraction of whole blood in the skin is ∼0.2%.[20] By incorporating 0.2% volume of our motility standard (i.e., phantom blood substitute) into the gelatin mixture, we simulated the volume fraction of whole blood in the tissue phantom. Dermal scattering simulation was achieved using a lipid emulsion solution that is biologically similar to the bilipid membrane of cells and organelles, which are the primary contributors to light scattering in skin tissue. We chose to neglect the effects of melanin in these experiments because

Table 1 Stress–strain relationship for the pressure settings used in the bench test.

Pressure amplitude (mmHg)	Expansion of tubing lumen (% volume change)
0	0.0
150	2.1
200	2.8
500	7.2
1000	14.6

melanin has a low overall concentration in the skin that varies widely based on skin tone.

Three different tissue phantoms were constructed according to the methods outlined by De Grand et al.[8] Briefly, 10% w/v type B gelatin (JT Baker, Center Valley, Pennsylvania) in Tris-buffered saline (pH 7.4; Alfa Aesar, Haverhill, Massachusetts) was mixed with a sterile 20% w/v intralipid fat emulsion (Baxter International, Deerfield, Illinois). Tissue phantoms with intralipid concentrations of 1%, 4%, and 6% were mixed. A concentration of 6% resulted in a tissue phantom that was opaque to the human eye. To the final mixture, the motility standard (0.2% of total volume) was added to approximate the volume fraction of whole blood in humans. The mixture was poured to a depth of 8 mm in a Petri dish with a single vessel submerged in the phantom. Once the tissue phantom had set, the phantom was connected to the pulsatile flow pump. The regions of tubing not immersed in the tissue phantom were covered with opaque cloth so that PPG measurements were collected only from tubing fully encased within the tissue phantom.

2.1.4 Optical characterization

To ensure the acquisition of any signal by the noncontact PPG imager was indeed true signal, PPG images were acquired of two 4% intralipid tissue phantoms under two different cases. In the first case, the motility standard was pumped through the tissue phantom at 60 bpm with 150-mmHg pressure. For the second case, 4% intralipid tissue phantom fluid was prepared and pumped through the tissue phantom at 60 bpm and 150 mmHg. PPG outputs were collected at a distance of 15 cm and then assessed. The outputs were used to determine if any resultant signal was due to the presence of motility standard flowing through the vessel and the accompanying volume change, or specular reflection and refractive index mismatch of the tissue phantom and associated tubing.

The optical properties of the tissue phantoms were also evaluated. Vis–NIR spectrophotometry was carried out on 1%, 4%, and 6% intralipid concentrations of the tissue phantom and the motility standard to assess how the attenuation coefficients compared. Given the limitations of the spectrophotometer, the observed attenuation coefficient is a combination of the scattering and absorptive properties of the media. Appropriate concentrations of the intralipid solutions were prepared and placed inside 1.0 cm × 1.0 cm plastic cuvettes (BrandTech Scientific Inc, Essex, Connecticut). The optical data were collected using a lamp, fiber, and spectrometer and processed using OceanView software (Ocean Optics, Dunedin, Florida). This data aimed to provide additional information on the optical qualities of the tissue phantom.

2.2 Photoplethysmography

2.2.1 Experimental photoplethysmography sensor

The PPG sensor in this investigation was the DeepView DVS 1000p (Spectral MD, Inc.). This system was comprised of a 12-bit 1025×512 pixel CMOS monochromatic imager (Photonis Lynx CMOS). The sensor contained square pixels of 5.6 μm length. The camera was connected via cable to a frame-grabber in a computer using a camera link in base mode. The camera was equipped with a 1/3 in. M12-mount lens with focal length 2.8 mm (f2.0). The camera collected frames at 30 frames per second using a rolling shutter.

The illumination source consisted of four 850-nm infrared light-emitting diodes (LEDs). Red and NIR light have historically been used for PPG systems since they maximize penetration for optical imaging techniques.[21] The LEDs were encased in glass lenses that produced a beam angle of 18 deg, and no cross-polarization was used. Each LED was driven by a DC current source at 150 mA, 100% duty cycle. The LEDs were mounted to the camera using a custom ballast. The ballast positioned the LEDs in a plane ~6 cm in front of the camera lens. In this plane, the LEDs were positioned perpendicular to the imaging target with their center of irradiance in each corner of the camera's field of view.

For the bench setup, the camera and illumination system were mounted on a rail system orthogonal to the imaging target on an optical bench. The working range for this instrument was 10 to 20 cm from the imaging target's surface. The data capture time was 27 s (800 total frames). A diagram of the experimental setup is shown in Fig. 1.

2.3 Data Collection

The bare-vessel and tissue phantoms were used to assess the ability of the noncontact PPG imaging system to detect a variety of parameters as described in Secs. 2.3.1–2.3.3.

The following equipment was used to collect measurements from the same bare-vessel and tissue phantoms: (1) a digital pressure transducer (Harvard Apparatus, Holliston, Massachusetts; Model# 60-3002, Serial# A-49918) directly measured the pressure changes in the fluid circuit; (2) a pulse oximeter with a wavelength of 910 nm (Nonin Medical, Plymouth, Minnesota; Avant 9600, Serial# 501387601) was used to detect PPG waveforms via direct contact.

2.3.1 Pulse pressure detection

Using the bare-vessel phantom, pulse pressure was varied from 0 to 1000 mmHg while pumping at a constant frequency of 60 bpm. We measured the response of the systems to the changing pulse pressures by measuring their power spectral density (PSD). The maximum value of the PSD at the frequency of the pump was determined for each pressure amplitude setting. The PSD was then calculated by taking the power spectrum of the time varying signal. The zero-pulse pressure (i.e., "no-flow" condition) was used as a negative control.

2.3.2 Pulse frequency detection

The ability of the noncontact PPG imager to detect pulsatile flow was assessed using both the bare-vessel and tissue phantoms. In the bare-vessel phantom, the frequency of the PPG waveform was varied by changing the frequency of the pump. The frequency was set to three values encompassing a physiologic range from bradycardia to tachycardia (40, 120, and 200 bpm), and the ability of each system to measure pulse frequency was then tested. To generate pulse frequency data from the noncontact PPG imager, a Fourier transform was applied to the time-domain waveform of the device. The result from the noncontact PPG imaging system was compared with that of the algorithm derived pulse oximeter.

The ability of the noncontact PPG imager to detect the pulse frequency in phantoms of varying intralipid concentrations (1%, 4%, and 6%) was also evaluated. Intralipid 1% solution has been described to accurately mimic skin tissue optical
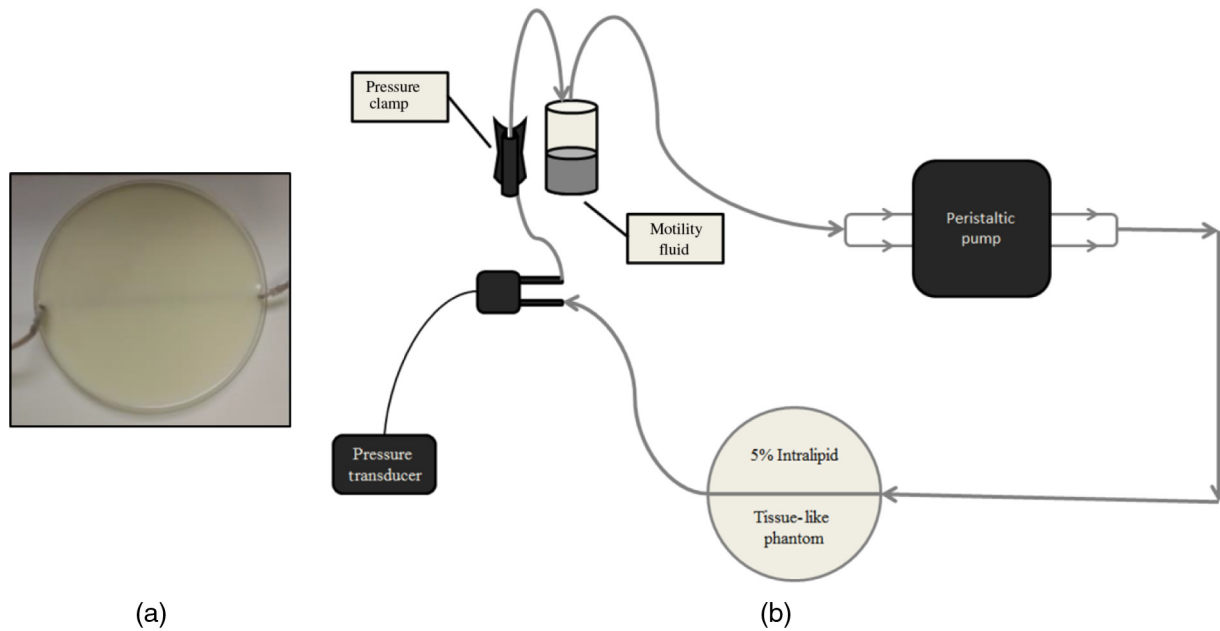
Fig. 1 (a) Tissue phantom in a Petri dish with an elastic tube embedded in the homogeneous tissue matrix, which mimics the blood flow under the skin. (b) The phantom apparatus is designed to simulate human pulsatile blood flow in a laboratory setting. The peristaltic pump drives the motility fluid through an elastic phantom vessel, 8.0 mm below the gelatin–intralipid tissue-like phantom matrix. Due to the elasticity of the tubing, an ∼2% volume expansion in the phantom vessel, similar to that of human arteries, occurs with each cycle of the peristaltic pump.

properties, including scattering.[7] However, the 1% concentration matrix did not visually conceal the embedded silastic tubing when filled with the motility standard. Therefore, we increased the intralipid concentration to 4% and 6% in order to better obscure the tube and motility standard during testing. The noncontact PPG imager was placed 15 cm from the target tissue phantom to detect the fluid flow signal in both single point mode and image mode. Fluid was pumped such that during each pump cycle a 2% volume change occurred in the embedded vessel phantom. Two-dimensional colormap images of the tissue phantom setup were acquired with the noncontact PPG imager: one in a no-flow condition to serve as a baseline control and another with the pump oscillating at a frequency of 60 bpm.

2.3.3 Spatial resolution

We assessed the spatial resolution of the noncontact PPG imager using the bare-vessel phantom set to a pulse pressure of 150 mmHg and frequency of 60 bpm. The distance from the imager to the bare-vessel phantom was incrementally increased from 10 to 20 cm while the signal strength and location were evaluated. Colormap outputs from the device were used to assess the ability of the imaging system to resolve the individual vessels.

2.4 Statistics and Calculations

PPG signal intensity was calculated on a pixel-by-pixel basis. Key steps for PPG signal and image processing are as follows (Fig. 2): (1) detrending to remove the DC wandering, (2) downsampling in time-domain to reduce the data volume, (3) filtering of the signal, (4) fast Fourier transformation converting time-resolved signal to frequency-domain, (5) extracting the spectral power, particularly at the frequency equivalent to the heart rate, (6) calculating the SNR, which is the ratio of the summation of intensity in heart rate band to the summation of the intensity in
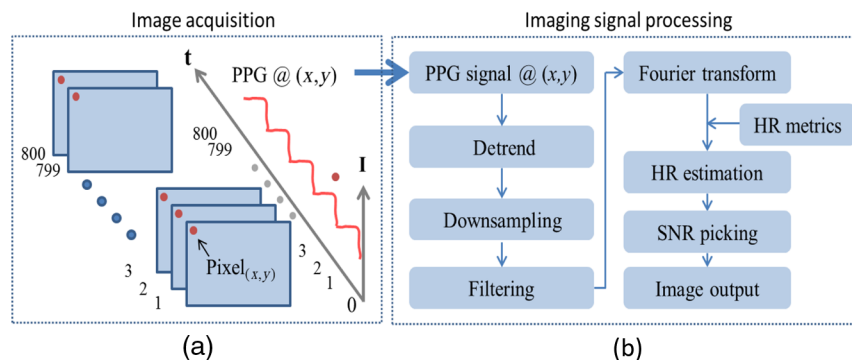

Fig. 2 Time-resolved PPG signal extraction. (a) Intensity at image pixel (x, y) is extracted sequentially from 800 contingent frames. (b) Processing method for quantifying PPG signals.
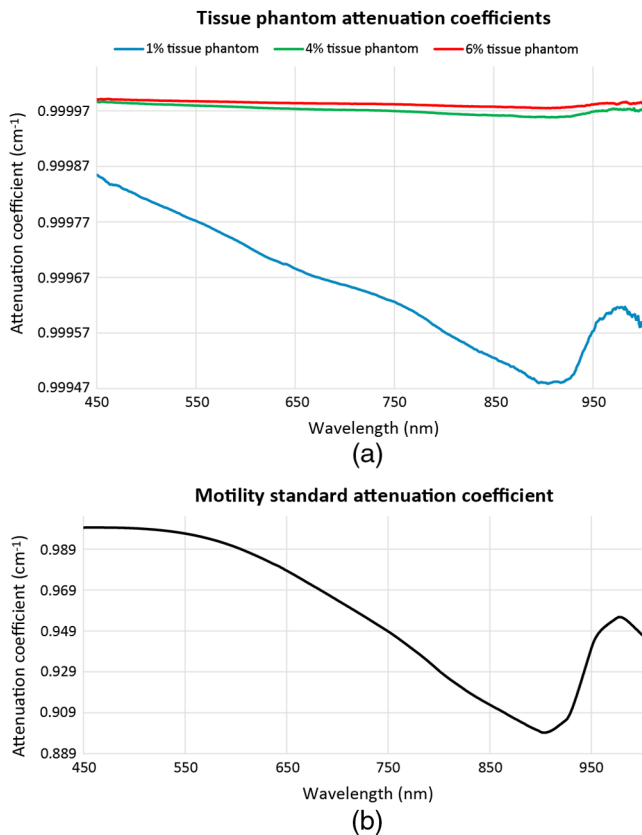
Fig. 3 (a) The attenuation coefficients of 1 cm samples of 1%, 4%, and 6% tissue phantoms and (b) the motility standard are shown. The motility standard, which mimics the absorption of blood, shows significant absorbance across the range and correlates with the spectrum observed from blood and hemoglobin. The tissue phantoms, which mimicked the properties observed in human skin, showed high levels of absorption across the range and increased as concentration increased.
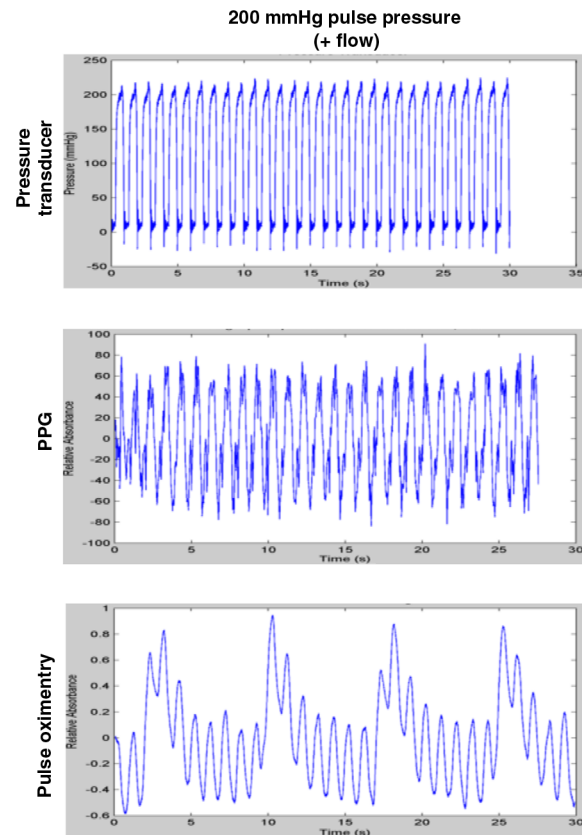

Fig. 4 Three devices were used to detect pulse pressure through the bare-vessel phantom at two settings: control setting of zero pressure with no-flow and 200-mmHg pulse pressure with positive flow at 60 bpm frequency. The pressure transducer and PPG imager system produced random noise under the initial control conditions, while pulse oximetry generated a low frequency regular DC offset signal at baseline. At the 200-mmHg pulse pressure setting, all three devices correctly detected signals that oscillated at the 60-bpm frequency of the pump. The pulse oximeter detected oscillations at 60 bpm that were superimposed over the same low frequency oscillation that was present in the control data.

higher frequency band (regarded as noise), and (7) using a color-map to represent each pixel's PPG SNR, yielding PPG image outputs. The colors were mapped linearly from lowest signal present to highest signal present relative to the values within a single image. Signal processing, statistical analysis, and comparisons were performed using MATLAB® software version 2012b (MathWorks, Natick, Massachusetts) and SigmaPlot 12.0 (Systat Software, San Jose, California).[4] Data collection from the pulse oximeter and pressure transducer devices was recorded with LabVIEW software (National Instruments, Austin, Texas).

3 Results

3.1 Optical Characterization

We investigated the source of the observed PPG signals from these tissue phantoms to determine whether the signals were simply a result of a refractive index mismatch between the tubing material and gelatin tissue phantom. Results showed that the PPG signals from the phantoms are indeed created by the 2% luminal volume increase, which the noncontact PPG imager is designed to identify and the phantoms are designed to mimic.

To further characterize the phantoms, we conducted vis–NIR spectrophotometry on tissue phantoms of varying intralipid

concentration and the motility standard. Again, given the limitations of the spectrophotometer used, the observed attenuation coefficients reflect both the scattering and absorptive properties of the media. The results showed that as intralipid concentration increased, the observed attenuation coefficient increased, which was to be expected (Fig. 3). The values were also within the range for tissues shown in the literature.[22,23] The coefficient for the motility standard across various wavelengths resembled that of hemoglobin, the predominant absorber of blood. These results confirmed the optical phantoms that were developed replicated the optical properties of tissue and its various components.

3.2 Pulse Pressure Detection

Using each imaging system, a no-flow (zero pressure) control measurement was acquired to establish each devices' baseline signal and account for the effect of noise in each imaging system. For the pressure transducer and noncontact PPG imager, the baseline signal was comparable to random noise effect. The signal acquired from pulse oximetry at baseline included a slight but regular, repetitive DC offset. The signals acquired
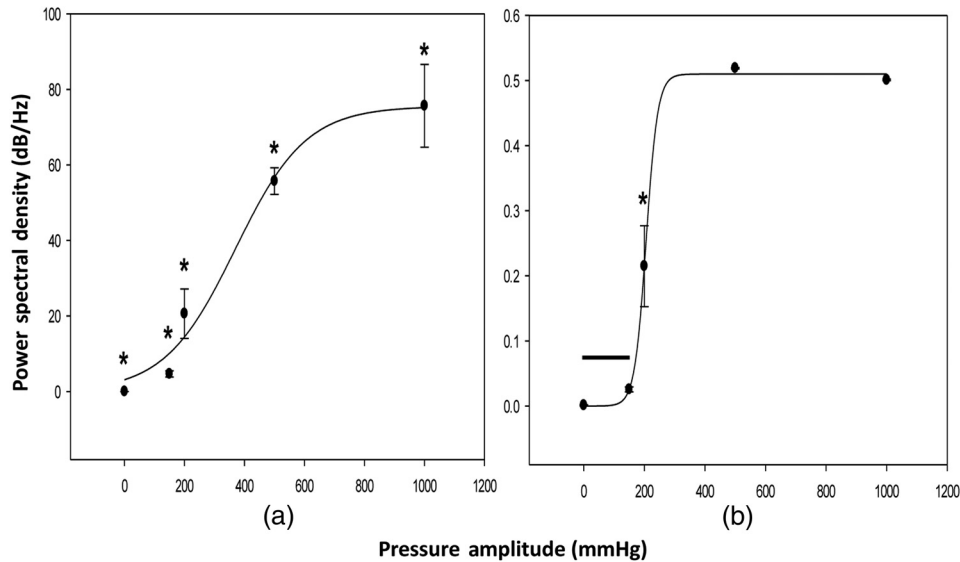
Fig. 5 PSD over a range of pressure amplitude settings as measured by (a) PPG imaging and (b) pulse oximetry. Pump frequency remained constant at 60 bpm throughout the test for each modality. Values marked with * are different with statistical significance as determined by one-way analysis of variance ($p < 0.05$). Values encompassed by a horizontal line are not significantly different from each other, but are different from values labeled with *. A sigmoid curve was fit to the data ($f = a/\{1 + \exp[-(x - x_0)/b]\}$) with $R > 0.98$ for both.

during the no-flow, control condition were then compared to the signals acquired with a pulse pressure of 150 mmHg oscillating at 60 bpm. The pulse pressure was detected by all of the devices as demonstrated by the oscillating signal strength at 60 bpm (Fig. 4). The signal produced by the pulse oximeter under these conditions was visible over the baseline repetitive DC offset detected under the no-flow, control conditions.

We then observed the PSD of the systems across a range of pulse pressures. For both the noncontact PPG imager and pulse oximeter, the system response showed an increase in signal amplitude with increasing pulse pressure in the range of 150 to 600 mmHg [Figs. 5(a) and 5(b)]. At lower pressures, <150 mmHg, the diameter of the tube is modulated by less than 1%. This modulation was below the lower limit of detection by the noncontact sensor. Once the modulated pressure surpassed 150 mmHg, the detected PPG signal increased rapidly with increasing pressures until an upper limit was reached.

3.3 Pulse Frequency Detection

To determine if the noncontact PPG imager measured the appropriate pulse frequency generated by the phantom, three different frequencies (40, 120, and 200 bpm) in the vessel phantom were tested. The signals detected by the noncontact PPG imager

uniformly contained the correct frequency of pulsatile fluid flow (Table 2).

We also assessed the ability of the noncontact PPG imaging system to detect the pulse frequency signal from tissue phantoms of varying intralipid concentrations. The imager did not record any signal in the no-flow control condition, but a signal was detected when the pump was turned on. The signal generated from the tissue phantom was dispersed across an area wider than the diameter of the silastic tubing, likely due to scattering of light by the intralipid solution. Despite this scattering effect, the location of the tube in the phantom was easily discernable. As the concentration of intralipid increased, the imager remained capable of detecting pulsatile flow through the phantoms. The strength of the PPG signals, however, did decrease with the increasing intralipid concentration (Fig. 6).

Single-point measurements were then taken from an area of the tissue phantom directly above the embedded tissue phantom vessel. The imager was capable of detecting fluid flow in the tissue phantom using a single-point measurement. After filtering of the single-point signals, the power spectrum for the noncontact PPG imager was calculated and plotted (Fig. 7). The noncontact PPG data intermittently revealed a low power but dominant frequency at ~8.3 Hz (500 bpm) that was also observed during the no flow condition. This signal was not

Table 2 Signal frequency detected by each system in the bare-vessel pulse frequency detection experiment.

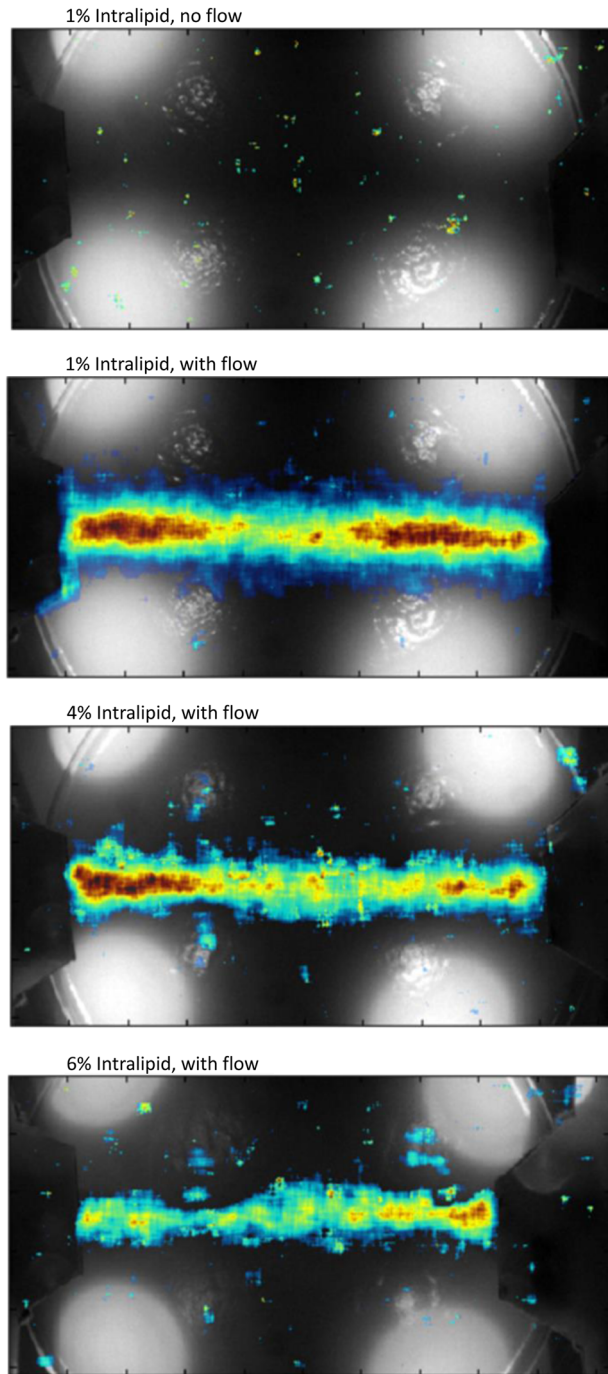| Pump setting (bpm)	Pulse oximetry (bpm)	Pressure monitor (bpm)	PPG (bpm)	LDI (bpm)
40	40	40.1 ± 0	40.1 ± 0.0	39.9 ± 0.1
120	120	120.2 ± 0	120.4 ± 0.0	119.9 ± 0.1
200	199	200.3 ± 0	200.9 ± 0.1	200.0 ± 0.0

Fig. 6 Flow images of the tissue phantom collected with the PPG imager. Test conditions are labeled above each pair of images. Flow was established at 60 bpm.

Fig. 7 Power spectra calculated from single-point data collected from varying tissue phantoms using the PPG imager.

consistently present, and because this frequency falls outside of the imager's working frequency range (40 to 200 bpm), the high frequency signal was ignored by the instrument's frequency detection algorithms. In active-flow testing, the imager detected the correct frequency (60 bpm) as evidenced by the peaks in power density at this frequency.

3.4 Spatial Resolution

At both test distances (10 and 20 cm), the imager detected the presence of simulated blood flow in the vessels (Fig. 8).
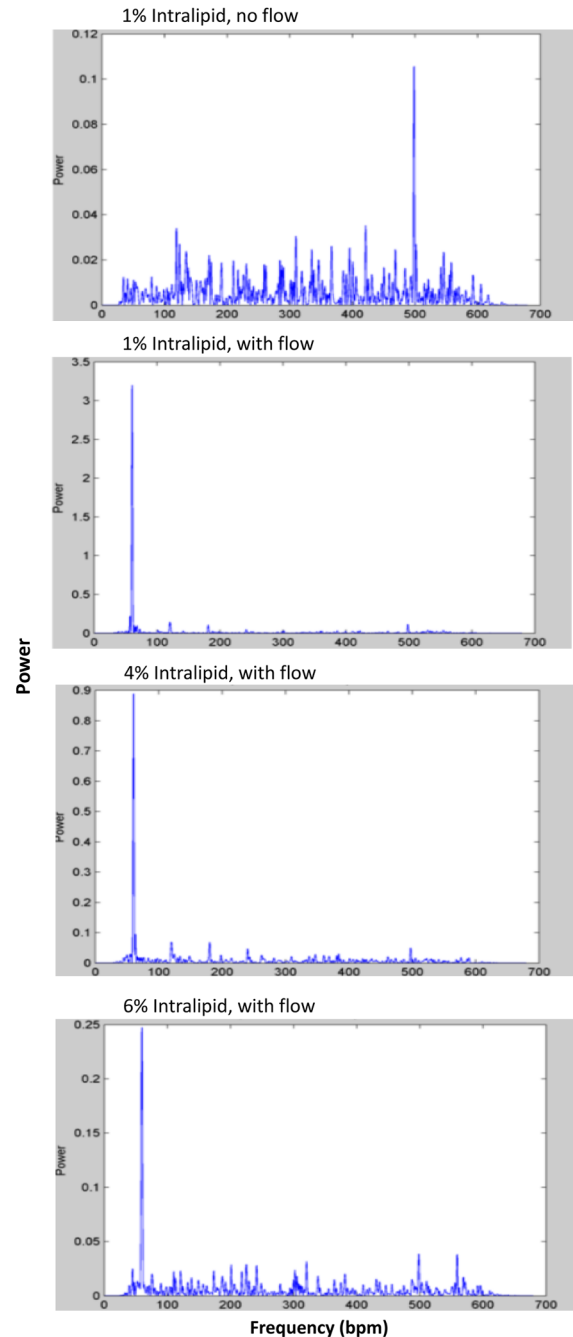
Furthermore, the colormap generated by the imager correctly overlaid the location of the parallel tubes. The imager could resolve the 5- and 10-mm spacing between tubes at both test distances, but the 1-mm spacing between tubes did not resolve at either test distance. The most significant contribution to the reduced spatial resolution of the noncontact PPG imager was the application of a spatial averaging filter (30×30 square) applied during preprocessing in exchange for smoothing of the signal from pixel-to-pixel. The imager also lost resolution in the periphery of its field of view at the test distance of 20 cm. This poor resolution was most likely due to a fish-eye distortion in the imager's lens.
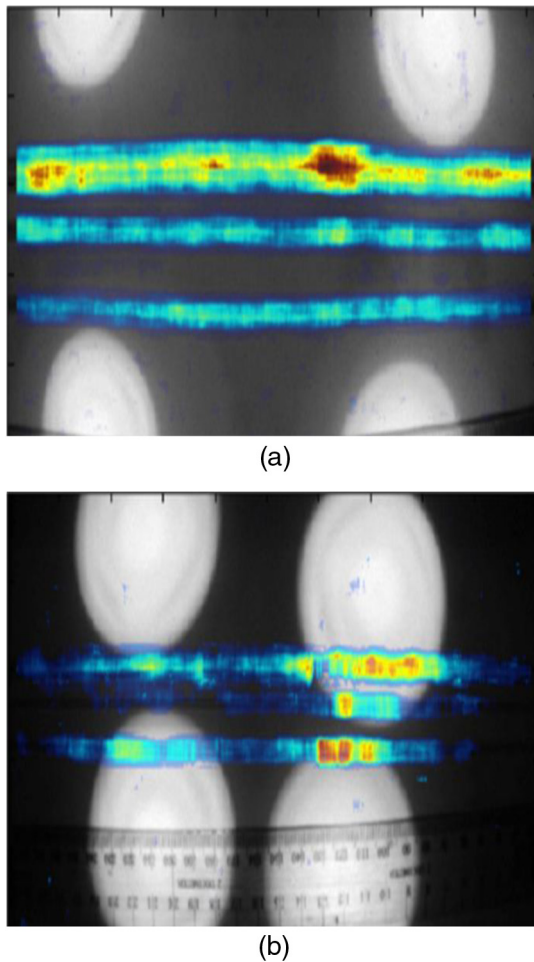
(a)

(b)

Fig. 8 PPG images taken at two distances from the bare-vessel phantoms to assess spatial resolution [(a) 10 cm and (b) 20 cm]. At all test distances, the PPG imager was able to detect flow patterns between tubes placed 5 and 10 mm apart but not between the tubes placed only 1 mm apart. At the 20-cm test distance, the PPG imager did not maintain this level of resolution along the periphery of its field of view.

4 Discussion and Conclusion

The results of our study are notable for several reasons. We have developed optical bare-vessel and tissue phantoms that mimic the dynamic physiology and microcirculatory blood flow of skin tissue. The time variant signal produced by the phantoms is innovative and provides wider applicability as a testing medium. Previous phantoms discussed in the literature were static and did not allow for the assessment of dynamic systems. These tissue phantoms can be used to evaluate not only non-contact PPG imaging systems but also other optical imaging systems under bench-top conditions. The construction of the phantoms is quick and adaptable. The optical properties of the phantoms can be tuned by researchers to mimic specific tissues or anatomical locations. The dynamic phantoms described can be used for the assessment of future optical imaging systems and the development of even more sophisticated phantoms.

Although our phantoms mimic the optical properties of tissue, they do not perfectly replicate the *in vivo* physiology, including the range of physiologic blood pressures. The high pressures used were a result of the tubing material being more rigid than human arteries. Another drawback of the

gelatin–intralipid phantom was the selected geometry for these experiments. Our blood vessel was placed 8.0 mm below the surface at the base of the mold. For this reason, we cannot rule out the effect of the boundary conditions at the base of the Petri dish, which would increase the backscattered photons because of the refractive index mismatch. The material on which the dish was placed would also impact the signal strength, because the polystyrene Petri dish does not absorb light in the NIR range.

After constructing tunable vessel and tissue phantoms capable of mimicking physiologic microcirculatory blood flow conditions, we tested the ability of the proposed noncontact PPG imager to detect pulsatile blood flow through these phantoms. The noncontact PPG imager was capable of detecting signal representatives of pulsatile flow through both the vessel and tissue phantoms at a variety of pulse pressurse and pulse frequencies with adequate spatial resolution. Moreover, the noncontact PPG imager was capable of translating this signal into colormaps of relative blood flow that accurately mapped the vessels' course through the tissue phantom model. These colormaps provide relevant information to clinicians in an easily digestible form. This highlights the ability of the noncontact PPG imager to produce valuable information for assessing tissue viability. Additional experiments showed the signals observed in the images are indeed true signals, attributable to the volume change caused by the motility standard (blood substitute) during pulsatile flow. Refractive index mismatch between the tubing and specular reflection from the surface of the model is not a contributor to the observed signal in our PPG imager.

Given the newly developed phantoms, noncontact PPG imaging systems can now be tested rapidly in a controlled, tunable environment that mimics properties of tissue. Future work will test the noncontact PPG imager in translational experiments on living animal or human models. Currently, physicians must rely on indirect, subjective evidence to assess microcirculatory blood flow in the skin. If the noncontact PPG imager can detect and map relative blood flow through the microcirculation of *in vivo* models, the system could provide useful information to clinicians regarding the relative viability of skin tissue. PPG imaging represents a potential solution to provide reliable, reproducible, quantitative information to healthcare providers regarding microcirculatory blood flow in the skin.

References

1. R. Moza, J. M. DiMaio, and J. Melendez, "Deep-tissue dynamic monitoring of decubitus ulcers: wound care and assessment," *IEEE Eng. Med. Biol. Mag.* **29**(2), 71–77 (2010).
2. J. E. Thatcher et al., "Multispectral and photoplethysmography optical imaging techniques identify important tissue characteristics in an animal model of tangential burn excision," *J. Burn Care Res.* **37**(1), 38–52 (2016).

3. D. R. King et al. "Surgical wound debridement sequentially characterized in a porcine burn model with multispectral imaging," *Burns* **41**, 1478–1487 (2015).

4. W. Li et al., "Outlier detection and removal improves accuracy of machine learning approach to multispectral burn diagnostic imaging," *J. Biomed. Opt.* **20**(12), 121305 (2015).

5. W. Verkuysse et al., "Calibration of contactless pulse oximetry," *Anesth. Analg.* **124**(1), 136–145 (2017).

6. M. Z. Poh, D. J. McDuff, and R. W. Picard, "Non-contact, automated cardiac pulse measurements using video imaging and blind source separation," *Opt. Express* **18**(10), 10762–10774 (2010).

7. B. W. Pogue and M. S. Patterson, "Review of tissue simulating phantoms for optical spectroscopy, imaging, and dosimetry," *J. Biomed. Opt.* **11**(4), 041102 (2006).

8. A. M. De Grand et al., "Tissue-like phantoms for near-infrared fluorescence imaging system assessment and the training of surgeons," *J. Biomed. Opt.* **11**(1), 014007 (2006).

9. S. Hu et al., "Development of effective photoplethysmographic measurement techniques: from contact to non-contact and from point to imaging," in *Conf. Proc. IEEE Engineering in Medicine and Biology Society*, pp. 6550–6553 (2009).

10. F. Corral, G. Paez, and M. Strojnik, "A photoplethysmographic imaging system with supplementary capabilities," *Opt. Appl.* **44**, 191–204 (2014).

11. J. G. Webster, *Design of Pulse Oximeters*, Medical Science Series, Institute of Physics Publishing, Bristol (1997).

12. M. Nitzan et al., "The variability of the photoplethysmographic signal: –a potential method for the evaluation of the autonomic nervous system," *Physiol. Meas.* **19**(1), 93–102 (1998).

13. I. Mizeva et al., "Quantifying the correlation between photoplethysmography and laser Doppler flowmetry microvascular low-frequency oscillations," *J. Biomed. Opt.* **20**(3), 037007 (2015).

14. I. Fredriksson et al., "Improved calibration procedure for laser Doppler perfusion monitors," *Proc. SPIE* **7906**, 790602 (2011).

15. T. Khamdaeng et al., "Arterial stiffness identification of the human carotid artery using the stress-strain relationship in-vivo," *Ultrasonics* **52**(3), 402–411 (2012).

16. R. J. Rodeheffer et al., "Exercise cardiac output is maintained with advancing age in healthy human subjects: cardiac dilatation and increased stroke volume compensate for a diminished heart rate," *Circulation* **69**(2), 203–213 (1984).

17. A. D. Mahon et al., "Evaluating the prediction of maximal heart rate in children and adolescents," *Res. Q. Exercise Sport* **81**(4), 466–471 (2010).

18. C. Giannattasio et al., "Large and medium sized artery abnormalities in untreated and treated hypothyroidism," *Eur. Heart J.* **18**(9), 1492–1498 (1997).

19. C. Giannattasio et al., "Fluctuations of radial artery distensibility throughout the menstrual cycle," *Arterioscler. Thromb. Vasc. Biol.* **19**(8), 1925–1929 (1999).

20. S. L. Jacques, "Skin optics," Oregon Medical Laser Center News, http://omlc.ogi.edu/news/jan98/skinoptics.html (1998).

21. J. E. Thatcher et al., "Imaging techniques for clinical burn assessment with a focus on multispectral imaging," *Adv. Wound Care* **5**(8), 360–378 (2016).

22. T. Lister, P. A. Wright, and P. H. Chappell, "Optical properties of human skin," *J. Biomed. Opt.* **17**(9), 090901 (2012).

23. S. Tseng, A. Grant, and A. J. Durkin, "In vivo determination of skin near-infrared optical properties using diffuse optical spectroscopy," *J. Biomed. Opt.* **13**(1), 014016 (2008).

C. Ikenna Nwafor received his BS degree in biomechanical engineering from Stanford University. He focuses on research and development of medical imaging systems as a biomedical engineer at Spectral MD, Inc.

Kevin D. Plant received his BS degree in biomedical engineering from the University of Texas at Austin. He is a biomedical engineer at Spectral MD, Inc.

Darlene R. King received her BS degree in mechanical engineering from the University of Texas at Austin and is a fourth year medical student at the University of Texas Southwestern. She is a biomedical engineer at Spectral MD, Inc.

Brian P. McCall received his BS degree in computer engineering from the University of Oklahoma and his PhD in optical engineering from Rice University. He is an imaging systems engineer at Spectral MD, Inc.

John J. Squiers received his BS degree in chemical engineering from Princeton University and his MD degree from the University of Texas Southwestern. He is currently a general surgery resident at Baylor University Medical Center. He focuses on clinical applications and clinical trial design as clinical specialist at Spectral MD, Inc.

Wensheng Fan received his MS degree in digital communication and signal processing from Northeastern University. He is the chief technology officer at Spectral MD, Inc. He is an executive, entrepreneur, and researcher with over 20 years of experience in natural speech recognition and real-time imaging systems.

J. Michael DiMaio received his MD degree from the University of Miami and completed his thoracic surgery residency at Duke. He is the founder and chief executive officer of Spectral MD, Inc. He serves as the director of postgraduate education and publications at Baylor Research Institute.

Jeffrey E. Thatcher received his PhD in biomedical engineering from the University of Texas Southwestern. He is the chief scientist at Spectral MD, Inc. where he oversees technology and applications research for medical imaging systems. His interests are in translational research of noninvasive imaging for wound care. His work in burn imaging was recognized by the 2015 Burke/Yannas award for original research in biomedical engineering form the American Burn Association.